

EFFECTS OF MAGNETIC FIELDS ON THE DISKOSEISMIC MODES OF ACCRETING BLACK HOLES

WEN FU AND DONG LAI

Department of Astronomy, Cornell University, Ithaca, NY 14853

Email: wenfu, dong@astro.cornell.edu

Draft version May 5, 2019

ABSTRACT

The origin of the rapid quasi-periodic variabilities observed in a number of accreting black hole X-ray binaries is not understood. It has been suggested that these variabilities are associated with diskoseismic oscillation modes of the black hole accretion disk. In particular, in a disk with no magnetic field, the so-called g-modes (inertial oscillations) can be self-trapped at the inner region of the disk due to general relativistic effects. Real accretion disks, however, are expected to be turbulent and contain appreciable magnetic fields. We show in this paper that even a weak magnetic field (with the magnetic energy much less than the thermal energy) can modify or “destroy” the self-trapping zone of disk g-modes, rendering their existence questionable in realistic black hole accretion disks. The so-called corrugation modes (c-modes) are also strongly affected when the poloidal field approaches equal-partition. On the other hand, acoustic oscillations (p-modes), which do not have vertical structure, are not affected qualitatively by the magnetic field, and therefore may survive in a turbulent, magnetic disk.

Subject headings: accretion: accretion disks — black hole physics — magnetic fields — X-ray: binaries — hydrodynamics — MHD

1. INTRODUCTION

In recent years, quasi-periodic variability has been observed from a number of Galactic compact X-ray binary systems. Of particular interest are several accreting black hole (BH) binaries which show pairs of quasi-periodic oscillations (QPOs) of fixed frequencies having ratios close to 2 : 3 (for example, GRO J1655-40 shows $f = 300, 450$ Hz; see Remillard & McClintock 2006 for a review). The origin of these QPOs is not understood. The fixed frequencies and frequency ratio led to the suggestion that these QPOs involve certain non-linear resonant phenomenon in the disk (e.g., coupling between the radial and vertical epicyclic oscillations of the disk fluid element; Kluzniak & Abramowicz 2002), but so far no fluid dynamical model producing these resonances has been developed (see Rebusco 2008 and references therein). Alternatively, it has been suggested that these QPOs may arise from acoustic oscillations in an accretion torus (Rezzolla et al. 2003; Lee, Abramowicz & Kluzniak 2004), with the oscillation frequencies determined by the (unknown) radial extent of the torus. Perhaps the theoretically most developed model for QPOs is the relativistic diskoseismic oscillation model (Kato & Fukue 1980; Okazaki et al. 1987; Nowak & Wagoner 1991; see Wagoner 1999; Kato 2001 for reviews), in which general relativistic (GR) effect produces trapped g-mode (also called inertial mode or inertial-gravity mode) oscillations in the inner region of the disk. Various theoretical issues related to this model have been studied, such as the role of corotational wave absorption (Kato 2003; Li, Goodman & Narayan 2003; Silbergleit & Wagoner 2007) and resonant mode excitations due to global disk deformation (Kato 2008; Ferreira & Ogilvie 2008).

The studies of the oscillation modes of disks/torii, such as those mentioned above, usually assume that the unperturbed flow is laminar and has no magnetic field. Real accretion disks, on the other hand, are highly turbulent due to the nonlinear development of magnetorotational instability (MRI) (see Balbus & Hawley 1998 for a review). The question therefore arises as to how the MRI-driven turbulence affects

the oscillation modes obtained from hydrodynamical models and to what extent these trapped modes remain “valid” in a realistic situation. Arras, Blaes & Turner (2006) attempted to address this issue by carrying out MHD simulations in the shearing-box geometry. They showed that axisymmetric standing sound waves give rise to distinct peaks in the temporal power spectrum, while inertial waves do not. The discrete frequencies obtained by them were due to the imposed periodic boundary conditions adopted in the simulations, and not due to any relativistic effect. Arras et al. suggested that their result poses a serious problem for QPO models based on g-modes (inertial waves). Recently, Reynolds & Miller (2008) reported on the results of global simulations of BH accretion disks (using Paczynski-Wiita pseudo-Newtonian potential) and showed that, while axisymmetric g-mode oscillations manifest in the hydrodynamic disk with no magnetic field, they disappear in the magnetic disk where MHD turbulence develops.

In this paper, we study analytically the effects of magnetic fields on the relativistic diskoseismic modes in accretion disks around BHs. We consider both poloidal and toroidal fields and use local analysis of the full MHD equations to examine how the magnetic field change the radial wave propagation diagrams for various modes. We show that the trapping region of g-modes can be easily “destroyed” even when the disk field strength is such that the associated Alfvén speed is much smaller than the sound speed. On the other hand, the propagation characteristics of p-modes (acoustic oscillations) and c-modes are largely unchanged. We summarize the basic MHD equations in §2 and review the properties of diskoseismic modes important for our analysis in §3. We examine in §4 and §5 the effects of poloidal field and toroidal field on those modes, respectively, and discuss the implications of our result in §6.

2. BASIC EQUATIONS

We consider a non-self-gravitating accretion disk, satisfying the usual ideal MHD equations:

$$\frac{\partial \rho}{\partial t} + \nabla \cdot (\rho \mathbf{v}) = 0, \quad (4)$$

$$\frac{\partial \mathbf{v}}{\partial t} + (\mathbf{v} \cdot \nabla) \mathbf{v} = -\frac{1}{\rho} \nabla \Pi - \nabla \Phi + \frac{1}{\rho} \mathbf{T}, \quad (5)$$

$$\frac{\partial \mathbf{B}}{\partial t} = \nabla \times (\mathbf{v} \times \mathbf{B}). \quad (6)$$

Here ρ , P , \mathbf{v} are the fluid density, pressure and velocity, Φ is the gravitational potential, and

$$\Pi \equiv P + \frac{B^2}{8\pi}, \quad \mathbf{T} \equiv \frac{1}{4\pi} (\mathbf{B} \cdot \nabla) \mathbf{B} \quad (7)$$

are the total pressure and the magnetic tension, respectively. The magnetic field \mathbf{B} also satisfies the equation $\nabla \cdot \mathbf{B} = 0$. We assume that the fluid obeys the barotropic equation of state $P = P(\rho)$.

We adopt the cylindrical coordinates (r, ϕ, z) which are centered on the central BH and have the z -axis in the direction perpendicular to the disk plane. The unperturbed background flow is assumed to be axisymmetric with a velocity field $\mathbf{v} = r\Omega(r)\hat{\phi}$, and magnetic field $\mathbf{B} = B_\phi(r)\hat{\phi} + B_z\hat{z}$, i.e., B_z is constant while B_ϕ has a radial dependence. Force balance in the unperturbed flow implies

$$\mathbf{G} \equiv \frac{1}{\rho} \nabla \Pi - \frac{1}{\rho} \mathbf{T} = \Omega^2 r \hat{r} - \nabla \Phi. \quad (8)$$

Consider perturbations of the form $e^{im\phi - i\omega t}$. The linearized fluid equations are

$$-i\tilde{\omega} \delta \rho + \frac{1}{r} \frac{\partial}{\partial r} (\rho r \delta v_r) + \frac{im\rho}{r} \delta v_\phi + \frac{\partial}{\partial z} (\rho \delta v_z) = 0, \quad (9)$$

$$-i\tilde{\omega} \delta v_r - 2\Omega \delta v_\phi = G_r \frac{\delta \rho}{\rho} - \frac{1}{\rho} \frac{\partial}{\partial r} \delta \Pi + \frac{1}{\rho} (\delta \mathbf{T})_r, \quad (10)$$

$$-i\tilde{\omega} \delta v_\phi + \frac{\kappa^2}{2\Omega} \delta v_r = -\frac{im}{\rho r} \delta \Pi + \frac{1}{\rho} (\delta \mathbf{T})_\phi, \quad (11)$$

$$-i\tilde{\omega} \delta v_z = G_z \frac{\delta \rho}{\rho} - \frac{1}{\rho} \frac{\partial}{\partial z} \delta \Pi + \frac{1}{\rho} (\delta \mathbf{T})_z, \quad (12)$$

$$-i\tilde{\omega} \delta B_r = \left(\frac{imB_\phi}{r} + B_z \frac{\partial}{\partial z} \right) \delta v_r, \quad (13)$$

$$-i\tilde{\omega} \delta B_\phi = -\frac{\partial}{\partial r} (B_\phi \delta v_r) + B_z \frac{\partial}{\partial z} \delta v_\phi - B_\phi \frac{\partial}{\partial z} \delta v_z + r \frac{d\Omega}{dr} \delta B_r, \quad (14)$$

$$-i\tilde{\omega} \delta B_z = -\frac{B_z}{r} \frac{\partial}{\partial r} (r \delta v_r) - \frac{imB_z}{r} \delta v_\phi + \frac{imB_\phi}{r} \delta v_z, \quad (15)$$

where

$$\tilde{\omega} = \omega - m\Omega \quad (16)$$

is the Doppler-shifted wave frequency, $\delta \rho$, $\delta \Pi$, $\delta \mathbf{v}$, $\delta \mathbf{B}$ are Eulerian perturbations, and ρ , \mathbf{B} refer to the unperturbed flow variables. In addition, for barotropic fluid, we have

$$\delta \rho = \frac{1}{c_s^2} \delta P = \frac{1}{c_s^2} (\delta \Pi - \frac{1}{4\pi} \mathbf{B} \cdot \delta \mathbf{B}), \quad (17)$$

where c_s is the sound speed.

To perform local (WKB) analysis, we consider perturbations with spatial dependence $e^{ik_r r + ik_z z}$. In the leading-order approximation, we keep only the radial gradient of $\Omega(r)$ and $B_\phi(r)$ while assuming that the variation scales of all the other background quantities are much larger than the wavelength of the perturbation, i.e., $k_r, k_z \gg 1/r$. The linearized MHD equations then reduce to

$$-\frac{i\tilde{\omega}}{\rho c_s^2} \delta \Pi + ik_r \delta v_r + ik_\phi \delta v_\phi + ik_z \delta v_z + \frac{i\tilde{\omega} B_\phi}{4\pi \rho c_s^2} \delta B_\phi + \frac{i\tilde{\omega} B_z}{4\pi \rho c_s^2} \delta B_z = 0, \quad (18)$$

$$-\frac{ik_r}{\rho} \delta \Pi + i\tilde{\omega} \delta v_r + 2\Omega \delta v_\phi + \left(\frac{ik_z B_z}{4\pi \rho} + \frac{ik_\phi B_\phi}{4\pi \rho} \right) \delta B_r - \frac{B_\phi}{2\pi \rho r} \delta B_\phi = 0, \quad (19)$$

$$-\frac{ik_\phi}{\rho} \delta \Pi - \frac{\kappa^2}{2\Omega} \delta v_r + i\tilde{\omega} \delta v_\phi + \frac{(q+1)B_\phi}{4\pi \rho r} \delta B_r + \left(\frac{ik_z B_z}{4\pi \rho} + \frac{ik_\phi B_\phi}{4\pi \rho} \right) \delta B_\phi = 0, \quad (20)$$

$$-\frac{ik_z}{\rho} \delta \Pi + i\tilde{\omega} \delta v_z + \left(\frac{ik_z B_z}{4\pi \rho} + \frac{ik_\phi B_\phi}{4\pi \rho} \right) \delta B_z = 0, \quad (21)$$

$$(ik_\phi B_\phi + ik_z B_z) \delta v_r + i\tilde{\omega} \delta B_r = 0, \quad (22)$$

$$ik_r B_\phi \delta v_r - ik_z B_z \delta v_\phi + ik_z B_\phi \delta v_z - p\Omega \delta B_r - i\tilde{\omega} \delta B_\phi = 0, \quad (23)$$

$$ik_r B_z \delta v_r + ik_\phi B_z \delta v_\phi - ik_\phi B_\phi \delta v_z - i\tilde{\omega} \delta B_z = 0, \quad (24)$$

where $k_\phi \equiv m/r$ and

$$\kappa^2 \equiv \frac{2\Omega}{r} \frac{d(r^2 \Omega)}{dr} \quad (25)$$

is the radial epicyclic frequency, and we have assumed $B_\phi \sim r^q$ and $\Omega \sim r^p$. Note that in deriving eqs. (15)-(21), we have dropped the terms proportional to G_r and G_z in eqs. (7) and (9): since $G_r = (\Omega^2 - \Omega_K^2)r \sim \Omega_K^2 r (H/r)^2$ and $G_z \sim \Omega_K^2 z$ (where Ω_K is the Keplerian frequency, i.e., the angular frequency in the absence of pressure force), G_r is much smaller than the other terms in eq. (7) provided that $k_r r \gg 1 + v_{A\phi}^2/c_s^2$, and G_z is also negligible if we focus on the mid-plane of the disk.

3. HYDRODYNAMIC LIMIT: DISKOSEISMIC MODES

In the absence of magnetic fields, the perturbed MHD equations (15)-(21) lead to the dispersion relation:

$$(\tilde{\omega}^2 - \kappa^2)(\tilde{\omega}^2 - k_z^2 c_s^2) = k_r^2 c_s^2 \tilde{\omega}^2. \quad (26)$$

For $k_z = 0$ (or $\tilde{\omega}^2 \gg k_z^2 c_s^2$), this becomes $\tilde{\omega}^2 = k_r^2 c_s^2 + \kappa^2$, the usual dispersion relation for spiral density wave; for $\tilde{\omega}^2 \ll k_z^2 c_s^2$, this becomes $\tilde{\omega} = \pm \kappa k_z / (k_r^2 + k_z^2)^{1/2}$, describing inertial oscillations (e.g., Goodman 1993).

For an accretion disk, with scale height $H \ll r$, the vertical dependence of the perturbation is not well described by the plane wave $e^{ik_z z}$ unless $k_z H \gg 1$. Okazaki et al. (1987) showed that for a thin disk, the perturbation equations can

be approximately separated in r and z (see also Nowak & Wagoner 1991, 1992; Ipser 1994). For example, for vertically isothermal disks with constant scale height H , one finds $\delta P(r, z), \delta v_r(r, z), \delta v_\phi(r, z) \propto H_n(z/H)$, while $\delta v_z(r, z) \propto H'_n(z/H)$, where $H_n(Z)$ (with $n = 0, 1, \dots$) is the Hermite polynomials and $H'_n(Z) = dH_n(Z)/dZ$. With this separation of variables, Okazaki et al. (1987) obtained the dispersion relation for a given n :

$$(\tilde{\omega}^2 - \kappa^2)(\tilde{\omega}^2 - n\Omega_\perp^2) = k_r^2 c_s^2 \tilde{\omega}^2, \quad (24)$$

where Ω_\perp is the vertical epicyclic frequency and is related to H by $H = c_s/\Omega_\perp$. An important property of relativistic disks around BHs is that κ is non-monotonic. Three types of trapped modes can be identified (see Fig. 1; see also Wagoner 1999, Kato 2001 and Ortega-Rodriguez et al. 2006 for reviews):

(i) P-modes. For $n = 0$, waves can propagate in the region where $\tilde{\omega}^2 > \kappa^2$. These are acoustic waves (modified by disk rotation), and have also been termed inertial-acoustic modes. If waves can be reflected at the disk inner radius (r_{ISCO} , the inner-most stable circular orbit), discrete p-modes can be self-trapped at the inner-most region of the disk (see Fig. 1a, 1c).

(ii) G-modes. For $n \geq 1$, waves can propagate in the region where $\tilde{\omega}^2 < \kappa^2 < n\Omega_\perp^2$ or $\tilde{\omega}^2 > \Omega_\perp^2 > \kappa^2$ (note that $\kappa < \Omega_\perp$ in GR). The former specifies the g-mode propagation zone: self-trapped g-modes can be maintained in the region where κ peaks (for $m = 0$: see Fig. 1b) or in the region where $\Omega - \kappa/m < \omega/m < \Omega + \kappa/m$ (for $m \neq 0$: see Fig. 1d).¹ Because these discrete, self-trapped modes do not require special boundary conditions (e.g., wave reflection at $r = r_{\text{ISCO}}$), they have been the focus of most studies of relativistic diskoseismology. Note that although we call these g-modes (following the terminology of Kato 2001 and Wagoner 1999), they have no relation to gravity waves, which are driven by buoyancy. Instead, these modes describe inertial oscillations, and have also been termed inertial modes (or inertial-gravity modes).

(iii) C-modes. For $n \geq 1$ and $m \geq 1$, the wave propagation condition $\tilde{\omega}^2 > n\Omega_\perp^2 > \kappa^2$ leads to an additional wave trapping region, where $\omega/m < \Omega - \sqrt{n}\Omega_\perp/m$ (see Fig. 1d). Note that for spinning BHs, $\Omega_\perp < \Omega$. Clearly, these modes exist only when $\Omega - \sqrt{n}\Omega_\perp/m > 0$ and wave reflection occurs at $r = r_{\text{ISCO}}$. Following the previous works (e.g., Kato 1990 and Silbergleit et al. 2001, who focused on the “fundamental” $n = m = 1$ mode, corresponding to the Lense-Thirring precession of the inner disk), we call these (“corrugation”) c-modes.

Comparing eqs. (23) and (24), we see that we can obtain the radial dispersion relation of different modes by adopting the vertical “quantization” condition $k_z = \sqrt{n}/H$ in eq. (23), with $k_z = 0$ specifying p-modes. In a generic disk (e.g., when the disk is not isothermal vertically), the same “quantization” condition would not hold, but we still expect $k_z \sim 1/H \sim \Omega_\perp/c_s$ for the (vertically) lowest-order g-mode or c-mode. In the next sections, we will adopt $k_z = \sqrt{\eta}\Omega_\perp/c_s$, with η of order unity, when we study how magnetic fields modify low-order g-modes and c-modes.

Our approach in this paper is based on Newtonian theory. GR effect can be incorporated into our analysis by using the Paczynski-Witta pseudo-Newtonian potential, $\Phi = -M/(r -$

¹ Note that non-axisymmetric g-modes with $\omega/m < \Omega(r_{\text{ISCO}})$ contain corotation resonance in the wave zone, leading to strong damping of the mode (Kato 2003; Li et al. 2003; Zhang & Lai 2006). On the other hand, modes with $\Omega(r_{\text{ISCO}}) < \omega/m < \max(\Omega + \kappa/m)$ do not suffer corotational damping, and are therefore of great interest.

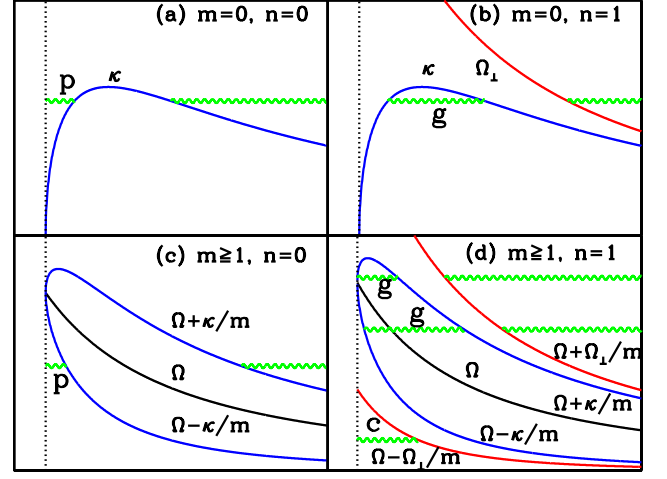


FIG. 1.— Wave propagation diagram showing various trapped modes in BH accretion disks: (a) axisymmetric p-mode; (b) axisymmetric g-mode; (c) non-axisymmetric p-mode; (d) non-axisymmetric g-mode and c-mode. The curves depict various critical frequencies (κ , $\sqrt{n}\Omega_\perp$, Ω , $\Omega \pm \kappa/m$, $\Omega \pm \sqrt{n}\Omega_\perp/m$), the vertical dotted lines denote the inner-most stable circular orbit (ISCO). The curvy horizontal lines specify wave propagation zones and the height of the line is ω (for the top panels) or ω/m (for the bottom panels) of the mode.

2M). Alternatively, we could simply replace the Newtonian Ω , Ω_\perp , κ by their exact general relativistic counterparts (e.g., Okazaki et al. 1987):

$$\Omega = \frac{\sqrt{M/r^3}}{1 + a\sqrt{M/r^3}}, \quad (25)$$

$$\Omega_\perp = \Omega \left[1 - \frac{4aM^{1/2}}{r^{3/2}} + \frac{3a^2}{r^2} \right]^{1/2}, \quad (26)$$

$$\kappa = \left[\frac{M(r^2 - 6Mr + 8aM^{1/2}r^{1/2} - 3a^2)}{r^2(r^{3/2} + aM^{1/2})^2} \right]^{1/2} \quad (27)$$

(in geometric units such that $G = c = 1$), where $a = J_s/M$ is the spin parameter of the black hole. In general, $\Omega \geq \Omega_\perp > \kappa$. In the case of a Schwarzschild BH, $\Omega = \Omega_\perp > \kappa$, with κ peaks at $r = 8M$ and becomes zero at $r_{\text{ISCO}} = 6M$. This non-monotonic behavior of the radial epicyclic frequency is preserved for Kerr BHs, and, as discussed above, is the key ingredient for the existence of trapped diskoseismic modes.

4. EFFECT OF POLOIDAL FIELDS

We first consider the case of a pure poloidal field, with $B_\phi = 0$. Equations (15)-(21) then lead the dispersion relation:

$$\begin{aligned} & \tilde{\omega}^6 - [(k_z^2 + k_r^2)(c_s^2 + v_{Az}^2) + k_z^2 v_{Az}^2 + \kappa^2] \tilde{\omega}^4 \\ & + \left\{ k_z^2 v_{Az}^2 \left[(k_z^2 + k_r^2)(2c_s^2 + v_{Az}^2) + \frac{d\Omega^2}{d \ln r} \right] + \kappa^2 k_z^2 c_s^2 \right\} \omega^2 \\ & - k_z^4 v_{Az}^2 c_s^2 \left[(k_z^2 + k_r^2) v_{Az}^2 + \frac{d\Omega^2}{d \ln r} \right] = 0, \end{aligned} \quad (28)$$

where $v_{Az} \equiv B_z/\sqrt{4\pi\rho}$. In the incompressible limit, this reduces to the dispersion relation found in, e.g., Balbus & Hawley (1991). For a given $\mathbf{k} = (k_r, k_\phi, k_z)$, equation (28) admits three branches, corresponding to fast, slow magnetosonic waves and Alfvén wave, all modified by differential rotation. For $k_z \gg k_r$, the Alfvén branch can become unstable when $k_z^2 v_{Az}^2 < -d\Omega^2/d\ln r$. This is the well-known MRI (e.g., Balbus & Hawley 1998).

4.1. P-modes

If $k_z = 0$, equation (28) reduces to

$$\tilde{\omega}^2 = \kappa^2 + k_r^2(c_s^2 + v_{Az}^2). \quad (29)$$

This is almost the same expression as in pure hydrodynamic case ($\tilde{\omega}^2 = \kappa^2 + k_r^2 c_s^2$), the only difference being that the sound speed is replaced by fast magnetosonic wave speed, $\sqrt{c_s^2 + v_{Az}^2}$. Thus the basic property of p-modes is not affected by poloidal magnetic fields.

4.2. G-modes

For a fixed $k_z = \sqrt{\eta}/H = \sqrt{\eta}\Omega_\perp/c_s$ (see §3), we can rewrite eq. (28) as an expression for k_r^2 :

$$(c_s^2 + v_{Az}^2)k_r^2 = \frac{(\tilde{\omega}^2 - \omega_1^2)(\tilde{\omega}^2 - \omega_2^2)(\tilde{\omega}^2 - \omega_5^2)}{(\tilde{\omega}^2 - \omega_3^2)(\tilde{\omega}^2 - \omega_4^2)}. \quad (30)$$

The five critical frequencies are given by

$$\omega_1^2 = \eta(\Omega_\perp)^2, \quad (31)$$

$$\omega_2^2 = \frac{1}{2} \left[\kappa^2 + 2\eta(\Omega_\perp)^2 b^2 + \sqrt{\kappa^4 + 16\eta(\Omega_\perp)^2 b^2} \right] \quad (32)$$

$$\omega_3^2 = \eta(\Omega_\perp)^2 b^2, \quad (33)$$

$$\omega_4^2 = \eta(\Omega_\perp)^2 \frac{b^2}{1+b^2}, \quad (34)$$

$$\omega_5^2 = \frac{1}{2} \left[\kappa^2 + 2\eta(\Omega_\perp)^2 b^2 - \sqrt{\kappa^4 + 16\eta(\Omega_\perp)^2 b^2} \right] \quad (35)$$

where $b \equiv v_{Az}/c_s$.

Equation (30) allows us to identify various wave propagation regions ($k_r^2 > 0$). We first consider subthermal fields, with $b < 1$. When $b \lesssim 0.4$ (and with $\eta = 1$ for the lowest order g-modes), the five critical frequencies satisfy $\omega_1^2 > \omega_2^2 > \omega_3^2 > \omega_4^2 > 0 > \omega_5^2$ in the inner region of the disk. Thus there are three wave propagation regions:

$$\text{Region I :} \quad \tilde{\omega}^2 > \omega_1^2, \quad (36)$$

$$\text{Region II :} \quad \omega_3^2 < \tilde{\omega}^2 < \omega_2^2, \quad (37)$$

$$\text{Region III :} \quad \tilde{\omega}^2 < \omega_4^2. \quad (38)$$

Region II corresponds to the original g-mode cavity modified by the magnetic field; in the zero field limit, $\omega_3 = 0$, $\omega_2 = \kappa$ and eq. (37) reduces to $\tilde{\omega}^2 < \kappa^2$. Fig. 2 depicts the critical frequencies ω_2 and ω_3 for several values of b . This also serves as the propagation diagram for $m = 0$ g-modes (wave can propagate in region where $\omega_3 < \omega < \omega_2$). We see that as the magnetic field increases, the g-mode self-trapping zone gradually shrinks and disappears even when the magnetic field is still very subthermal (for a Schwarzschild BH, this occurs for $b \gtrsim 0.08$). More precisely, the g-mode cavity can still exist for large b , but it now requires a reflection boundary at

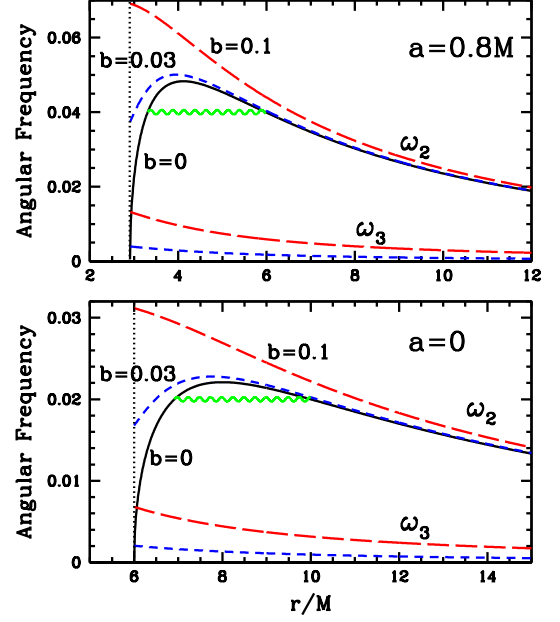


FIG. 2.— The effect of poloidal magnetic field on the g-mode propagation zone for $m = 0$, $\eta = 1$. In each panel, the upper three curves are ω_2 (eq. [32]) and the lower two curves are ω_3 (eq. [33]). Axisymmetric g-modes of frequency ω can propagate in the region where $\omega_3 < \omega < \omega_2$. The solid line refers to the case of $b = 0$, the short-dashed line $b = 0.03$ and the long-dashed line $b = 0.1$, where $b \equiv v_{Az}/c_s$, with $v_{Az} = B_z/\sqrt{4\pi\rho}$ (Alfvén speed) and c_s the sound speed. The vertical dotted lines correspond to the inner disk radius at ISCO. The curly horizontal lines specify the wave propagation zones, and the height of the line is ω of the mode. The lower and upper panels are for the case of a Schwarzschild BH ($a = 0$) and a Kerr BH ($a = 0.8M$), respectively. The angular frequencies are in units of $M^{-1} = c^3/(GM)$.

r_{ISCO} . This behavior can be easily understood by inspecting eq. (32): While κ peaks at some radius r_{max} , Ω_\perp and Ω both increase monotonically with decreasing r . Since Ω_\perp and Ω are much larger than κ in the inner region of the disk, the $2(\Omega_\perp b)^2$ term or the $4\Omega_\perp \Omega b$ term can dominate over κ^2 even when b is still small, therefore making the self-trapping zone disappear. Roughly, this occurs at $b \gtrsim b_{\text{crit}} \sim (\kappa^2/2\Omega_\perp \Omega)_{r_{\text{max}}}$.

For non-axisymmetric perturbations ($m \neq 0$), the wave propagation region II is determined by (i) $\Omega - \omega_2/m < \omega/m < \Omega + \omega_2/m$, and (ii) $\omega/m > \Omega + \omega_3/m$ or $\omega/m < \Omega - \omega_3/m$. Fig. 3 shows the propagation diagram. As mentioned before (see Footnote 1), for $b = 0$, only the modes with $\omega > m\Omega(r_{\text{ISCO}})$ are of interest, since otherwise there is a corotation resonance in the wave zone, leading to strong mode damping (Kato 2003; Li, Narayan & Goodman 2003; Zhang & Lai 2006). Thus, self-trapped g-modes reside around the radius where $\Omega + \omega_2/m$ is the maximum (and this maximum arises because κ depends nonmonotonically on r). We see from Fig. 3 that this g-mode self-trapping region disappears as b increases. The larger m is, the more fragile is the cavity. For example, the $m = 1$ cavity disappears for $b \gtrsim 0.015$, while for $m = 2$, this occurs for $b \gtrsim 0.005$.

4.3. C-modes

For $m \neq 0$ and $\eta \sim 1$, equation (30) also describes trapped c-modes. When $b \lesssim 0.4$, ω_1^2 is the largest among all the critical frequencies and the c-mode propagation zone corresponds to Region I (see eq. [36]). Note that since ω_1 is not affected by the magnetic field, the trapping region is deter-

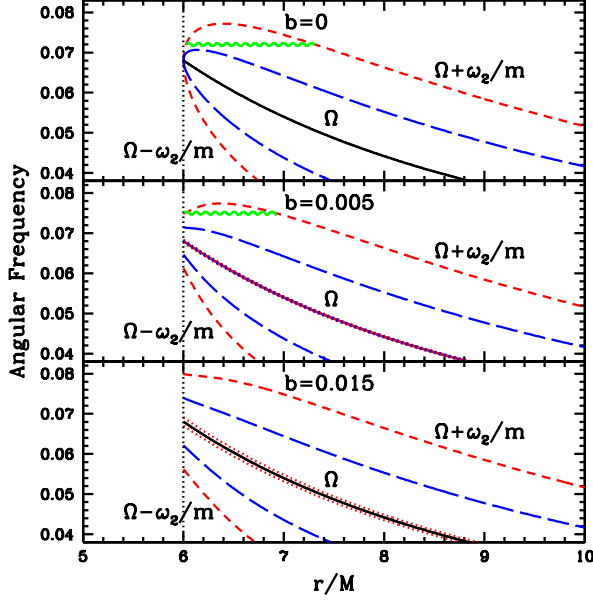


FIG. 3.— The effect of poloidal magnetic field on the g-mode propagation zone for $m \neq 0, \eta = 1, a = 0$. The three panels are for $b = v_{Az}/c_s = 0, 0.005$ and 0.015 . The solid line, short-dashed lines and the long-dashed lines show Ω , $\Omega \pm \omega_2$ and $\Omega \pm \omega_2/2$, respectively. In the bottom panel, the dotted lines show $\Omega \pm \omega_3$ (In the upper and middle panels, $\Omega \pm \omega_3$ almost coincide with Ω , since $\omega_3 = 0$ for $b = 0$ and $\omega_3 \ll \Omega$ for $b \ll 1$). Non-axisymmetric g-modes can propagate in the region where $\Omega - \omega_2/m < \omega/m < \Omega - \omega_3/m$ or $\Omega + \omega_3/m < \omega/m < \Omega + \omega_2/m$. The vertical dotted lines correspond to the inner disk radius at ISCO. The curvy horizontal lines in top and middle panels specify wave propagation zones and the height of the line is ω/m of the mode. Note that the self-trapping zone (depicted in the upper and middle panels) disappears as b increases. The angular frequencies are in units of $M^{-1} = c^3/(GM)$.

mined by $\omega/m < \Omega - \omega_1/m = \Omega - \Omega_\perp/m$ (for $\eta = 1$, see the upper panel of Fig. 4; cf. Fig. 1d). When $b \gtrsim 0.4$, the ordering between ω_1 and ω_2 switches and c-modes propagate in the region where $\tilde{\omega}^2 > \omega_2^2$, with the trapping zone determined by $\omega/m < \Omega - \omega_2/m$ (see the bottom panel of Fig. 4). Thus, in the presence of a reflection boundary at r_{ISCO} , c-modes are not affected by the poloidal magnetic field when $b \lesssim 0.4$, but can be appreciably modified when $b \gtrsim 0.4$.

From eq. (30) we can identify other wave propagation zones (see eq. [38]). Fig. 5 gives an example, for $m = 2, b = 0.7$. Note that, except for the c-mode trapping zone discussed above, all the propagation zones are bounded by at least one “singular point” (where $k_r \rightarrow \infty$). Unlike the turning point ($k_r \rightarrow 0$) associated with wave reflection, wave absorption is expected to occur at these singular points (see Zhang & Lai 2006; Tsang & Lai 2008a and references therein). Thus, the new wave trapping regions given by eq. (38) will not lead to interesting global oscillation modes (Note that in the case of $b = 0.7$, the ordering of five critical frequencies is different from the one described in §4.2. However, our conclusion still holds true, i.e., there is no chance to form a wave trapping zone bounded by two reflection points other than the c-mode oscillation region, which is bounded by a reflection point and the ISCO).

5. EFFECT OF TOROIDAL FIELDS

In this section, we consider the effect of a pure toroidal field, with $B_z = 0$. Various instabilities may exist for such field geometry, depending upon the rotation profile $\Omega(r)$ and the magnetic field profile $B_\phi(r)$ (e.g., Acheson & Gibbons 1978;

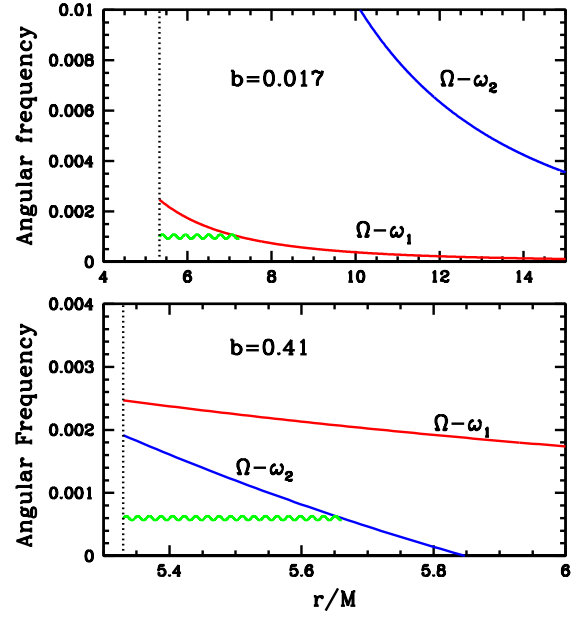


FIG. 4.— The effect of poloidal magnetic field on c-modes with $m = 1$ and $a = 0.2M$. The upper panel shows the original c-modes since b is small and $\omega_1 = \Omega_\perp$; in the bottom panel, with a large b , the c-mode trapping zone is instead bounded by the inner reflection boundary and $\Omega - \omega_2$. The vertical dotted line refers to the inner disk radius at ISCO. The curvy horizontal lines specify wave propagation zones and the height of the line is ω of the mode.

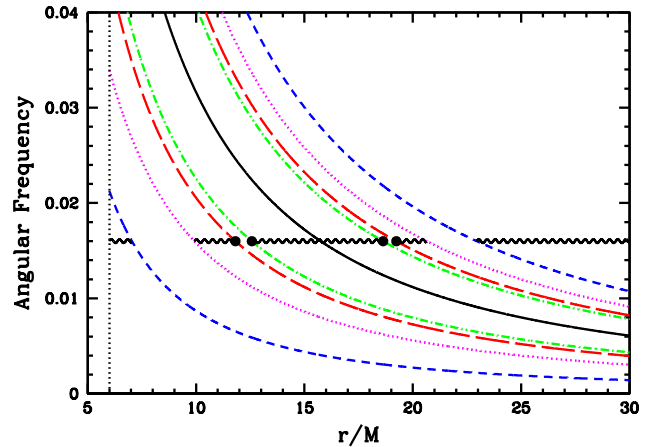


FIG. 5.— Wave propagation diagram for non-axisymmetric g-modes and c-modes, for $b = v_{Az}/c_s = 0.7, m = 2, \eta = 1$, and $a = 0$. The solid line, dot-short dashed lines, long-dashed lines, dotted lines and short-dashed lines show Ω , $\Omega \pm \omega_4/2$, $\Omega \pm \omega_3/2$, $\Omega \pm \omega_1/2$ and $\Omega \pm \omega_2/2$ (eqs. [31]–[34]), respectively. The vertical dotted line shows the inner disk radius. The curvy horizontal lines specify wave propagation zones and the height of the line is $\omega/2$ of the mode. The singular points (where $k_r \rightarrow \infty$) are indicated by filled circles. The angular frequencies are in units of $M^{-1} = c^3/(GM)$.

Terquem & Papaloizou 1996). Here we focus on how B_ϕ affects the diskoseismic modes.

5.1. *P-modes*

With $k_z = 0$, equations (15)-(21) reduces to

$$\tilde{\omega}^2 = \kappa^2 + k_r^2(c_s^2 + v_{A\phi}^2), \quad (39)$$

where $v_{A\phi} \equiv B_\phi / \sqrt{4\pi\rho}$. Thus, the toroidal field affects p-modes in the same way as the poloidal field does (see §4.1).

5.2. *G-modes*

Since the general dispersion relation for $m \neq 0$ is quite complicated, here we focus on axisymmetric perturbations.² With $m = 0$, Equations (15)-(21) lead to

$$\begin{aligned} \omega^4 - [\kappa^2 + (k_z^2 + k_r^2)(c_s^2 + v_{A\phi}^2)]\omega^2 + \kappa^2 k_z^2(c_s^2 + v_{A\phi}^2) \\ + 2(1-q)v_{A\phi}^2 c_s^2 k_z^2 / r^2 = 0, \end{aligned} \quad (40)$$

where $q = d \ln B_\phi / d \ln r$. Solving for k_r^2 , we have

$$k_r^2 = \frac{(\omega^2 - \omega_+^2)(\omega^2 - \omega_-^2)}{(c_s^2 + v_{A\phi}^2)\omega^2}, \quad (41)$$

with the two critical frequencies given by

$$\begin{aligned} \omega_\pm^2 = \frac{\kappa^2 + \eta \Omega_\perp^2 (1 + b_\phi^2)}{2} \pm \\ \frac{1}{2} \sqrt{[\kappa^2 - \eta \Omega_\perp^2 (1 + b_\phi^2)]^2 - 8(1-q)\eta v_{A\phi}^2 \Omega_\perp^2 / r^2}, \end{aligned} \quad (42)$$

where $b_\phi \equiv v_{A\phi} / c_s$ and we have used $k_z = \sqrt{\eta} / H = \sqrt{\eta} \Omega_\perp / c_s$ as in §4. Clearly, for $b_\phi = 0$, eq. (42) reduces to eq. (24).

When $q = 1$ (i.e., $B_\phi \propto r$), eq. (42) gives $\omega_+^2 = \eta(\Omega_\perp)^2(1 + b_\phi^2)$, and $\omega_-^2 = \kappa^2$. Since ω_-^2 is independent of B_ϕ , the g-mode propagation zone is unaffected no matter how strong the field is. When $q \neq 1$, as long as $v_{A\phi} \ll \Omega_\perp r$ (which is valid in most disk situations), the $8(1-q)\eta v_{A\phi}^2 \Omega_\perp^2 / r^2$ term in eq. (42) represents only a small correction, i.e., ω_-^2 is still very close to κ^2 . Thus for general toroidal field satisfying $v_{A\phi} \ll \Omega_\perp r$, the axisymmetric g-mode propagation zone is not affected by the magnetic field.

6. SUMMARY AND DISCUSSION

In this paper we have studied the effects of both poloidal and toroidal magnetic fields on the diskoseismic modes in BH accretion disks. Previous works by Kato, Wagoner and others have been based on hydrodynamic disks with no magnetic

field. The key finding of our paper is that the g-mode self-trapping zone (which arises from GR effect) disappears when the disk contains even a small poloidal magnetic field, corresponding to $v_{Az}/c_s = 0.01 - 0.1$ (see Fig. 2-3; v_{Az} is the Alfvén speed and c_s is the sound speed). It is well-known that the combination of a weak poloidal field and differential rotation gives rise to MRI, making real astrophysical disks turbulent. Numerical simulations indicate that the magnetic field grows as MRI develops, until it saturates at $v_{Az}/c_s \sim 1$ (i.e., the magnetic energy reaches equal-partition with the thermal energy; see, e.g., Balbus & Hawley 1998), much larger than the critical field strength needed to “destroy” the g-mode self-trapping zone. Thus, the g-mode properties (including the frequencies and excitations) derived from hydrodynamical models are unlikely to be applicable to real BH accretion disks. The disappearance of the g-mode trapping zone might also explain why Arras et al. (2006) and Reynolds & Miller (2008) did not see any global g-modes in their MHD simulations.

As mentioned in §1, g-mode oscillations have been considered a promising candidate to explain QPOs in BH X-ray binaries. Theoretically, these modes are appealing because in hydrodynamic disks their existence depends on general relativistic effect and does not require special disk boundary conditions. Our analytical results presented in this paper, together with recent numerical simulations (Arras et al. 2006; Reynolds & Miller 2008), suggest that magnetic fields and turbulence associated with real accretion disks can change this picture significantly.

While g-modes can be easily modified or “destroyed” by magnetic fields, our analysis showed that p-modes are not affected qualitatively. The magnetic field simply changes the sound speed to the fast magnetosonic wave speed and leaves the p-mode propagation diagram unchanged. We also showed that a weak poloidal field ($v_{Az}/c_s \ll 1$) does not affect the c-mode propagation zone, although a stronger field modifies it. Our results therefore suggests that global p-mode oscillation is robust and may exist in real BH accretion disks, provided that partial wave reflection at the disk inner edge can be achieved.³ Of particular interest is the non-axisymmetric p-modes, since they may be excited by instabilities associated with corotation resonance (Tsang & Lai 2008a, b).

We thank David Tsang for useful discussion. This work has been supported in part by NASA Grant NNX07AG81G and by NSF grant AST 0707628.

² Since c-modes necessarily require $m > 0$, our analysis here cannot be applied to c-modes.

³ Kato (2001) has discussed why such reflection may be possible.

REFERENCES

- Acheson, D. J. & Gibbons, M. P., 1978, Phil. Trans. Roy. Soc. Lond. A 289, 459
 Arras, P., Blaes, O. & Turner, N. J., 2006, ApJ, 645, L65
 Balbus, S. A. & Hawley, J. F., 1991, ApJ, 376, 214
 Balbus, S. A. & Hawley, J. F., 1998, Rev. Mod. Phys., 70, 1
 Ferreira, B. T. & Ogilvie, G. I., 2008, MNRAS in press (arXiv:0803.1671)
 Goodman, J., 1993, ApJ, 406, 596
 Ipser, J. R., 1994, ApJ, 435, 767
 Kato, S. & Fukue, J., 1980, PASJ, 32, 377
 Kato, S., 1990, PASJ, 42, 99
 Kato, S., 2001, PASJ, 53, 1
 Kato, S., 2003, PASJ, 55, 257
 Kato, S., 2008, PASJ, 60, 111
 Kluzniak, W. & Abramowicz, M. A., 2002, preprint (astro-ph/0203314)
 Lee, W. H., Abramowicz, M. A. & Kluzniak, W., 2004, ApJ, 603, L93
 Li, L. X., Goodman, J. & Naryan, R., 2003, ApJ, 593, 980
 Nowak, M. A. & Wagoner, R. V., 1991, ApJ, 378, 656
 Nowak, M. A. & Wagoner, R. V., 1992, ApJ, 393, 697
 Okazaki, A. T., Kato, S. & Fukue, J., 1987, PASJ, 39, 457
 Ortega-Rodriguez, M., Silbergleit, A. S. & Wagoner, R. V., 2006, preprint (astro-ph/0611101)

- Rebusco, P., 2008, To appear in New Astronomy Review, Proceedings of "Jean-Pierre Lasota, X-ray binaries, accretion disks and compact stars" (October 2007); Ed. M. Abramowicz (arXiv:0801.3658)
- Remillard, R. A. & McClintock, J. E., 2006, ARAA, Vol. 44, Issue 1, pp. 49-92
- Reynolds, C. S. & Miller, M. C., 2008, ApJ, submitted (arXiv:0805.2950)
- Rezzolla, L., Yoshida, S., Maccarone & Zanotti, O., 2003, MNRAS, 344, L37-L41
- Silbergleit, A. S., Wagoner, R. V. & Ortega-Rodriguez, M., 2001, ApJ, 548, 335
- Silbergleit, A. S. & Wagoner, R. V., 2007, ApJ, submitted (arXiv:0711.4848)
- Terquem, C. & Papaloizou, J. C. B., 1996, MNRAS, 279, 767
- Tsang, D. & Lai, D., 2008a, MNRAS, 387, 446
- Tsang, D. & Lai, D., 2008b, MNRAS, to be submitted
- Wagoner, R. V., 1999, Phys. Rep., 311, 259
- Zhang, H. & Lai, D., 2006, MNRAS, 368, 917